Dynamics around non-spherical symmetric bodies: II. The case of a prolate body

T. Ribeiro, O. C. Winter, G. Madeira, S. M. Giuliatti Winter

Monthly Notices of the ROYAL ASTRONOMICAL SOCIETY

MNRAS **525,** 44–56 (2023) https://doi.org/10.1093/mnras/stad2362
Advance Access publication 2023 August 4

Dynamics around non-spherical symmetric bodies: II. The case of a prolate body

T. Ribeiro [1]★ O. C. Winter,[1] G. Madeira [1,2] and S. M. Giuliatti Winter[1]

[1]*Grupo de Dinâmica Orbital and Planetologia, São Paulo State University -UNESP, Av. Ariberto Pereira da Cunha, 333, Guaratinguetá, SP 12516-410, Brazil*
[2]*Université de Paris, Institut de Physique du Globe de Paris, CNRS, F-75005 Paris, France*

Accepted 2023 July 25. Received 2023 July 25; in original form 2022 December 22

ABSTRACT

Dynamic exploration around non-spherical bodies has increased in recent decades due to the interest in studying the motion of spacecraft orbits, moons, and particle ring around these bodies. The dynamic structure around these objects is defined by regular and chaotic regions. The Poincaré surface of section technique allows mapping these regions, identifying the location of resonances, and the size of regular and chaotic zones, thus helping us to understand the dynamics around these bodies. Using this technique, we map in the *a*–*e* space the stable and unstable regions around ellipsoidal bodies, such as the dwarf planet Haumea, the centaur Chariklo, and other five hypothetical bodies, in which we keep part of the physical parameters of Haumea but we varied its period of rotation and ellipticity, to analyse the impact of these alterations in the extensions of the stable and unstable regions due to first kind orbits and spin-orbit type resonances. We identified a large region of stability, in semimajor axis and eccentricity, due to the first kind orbits. Periodic orbits of the first kind are present in a large semimajor axis interval for all considered systems and have almost zero eccentricity, while resonant and quasi-periodic orbits have high eccentricities. Furthermore, we identified the bifurcation of the 2:6 resonance when there is a spin reduction of a body with the same physical parameters as Haumea. This bifurcation generates a chaotic region, reducing the extension of the stability zone.

Key words: celestial mechanics – Kuiper belt objects: individual: (136108) Haumea – minor planets, asteroids: general – planets and satellites: dynamical evolution and stability.

1 INTRODUCTION

With the increasing discoveries of small non-spherical bodies, such as asteroids, centaurs, comets, and trans-Neptunian objects, the interest in understanding the dynamics of regions around these bodies, subjected to non-spherical gravitational potentials, has increased. This is because the orbits around these bodies generally differ from the Keplerian orbits of the two-body problem (Hu & Scheeres 2004; Ribeiro et al. 2021), as irregularities in their shape cause disturbances in their gravitational fields. To study the dynamics around these bodies, through numerical simulations, it is necessary to use physical models that adequately represent their shapes. Modelling by triaxial and Jacobi ellipsoids or the Maclaurin spheroid are widely used because they demand lower computational costs and they are good approximations for symmetrical and non-spherical bodies. The Maclaurin spheroid consists of a body with an equatorial radius A different from the polar radius C, the triaxial ellipsoid is formed by three semi-axes with different sizes, $A > B > C$, and the Jacobi ellipsoid is an ellipsoid triaxial that revolves around the minor axis (Chandrasekhar 1942). However, other modelling methods are needed for bodies with more irregular shapes, as the case of the asteroid Kleopatra. The Mascons model, developed by Geissler et al. (1996), and the Polyhedra model, created by Werner (1994), are capable of representing the surface contours of these objects with better precision, however, they demand higher computational costs.

The relevance of this type of dynamic exploration is justified by the interest in studying the motion of spacecraft orbits, moons, and ring particles around these bodies. Celestial bodies that can be modelled using ellipsoids or spheroids, the gravitational field can be studied by adding spherical harmonics. For oblate spheroids, the terms J_n are included, for example, J_2, J_4, and J_6, which correspond to the oblateness of the poles. For prolate ellipsoids, in addition to J_n, the term C_{22} is also added, which is related to the ellipticity in the equatorial region of the body. The effect of the gravitational potential generated by oblate spheroids is well known due to extensive studies of the dynamics of planetary rings and the orbits of artificial satellites, since planets with orbital rings in the solar system, such as Saturn, are oblate spheroids and, in the case of orbits of near Earth artificial satellites, it its necessary to take into account is oblateness of the planet. The same does not occur for prolate bodies, since the inclusion of the ellipticity term in the gravitational potential, produces effects that have been observed in recent decades, as in Hu & Scheeres (2004), which, intending to study the motion of a spacecraft around the equator of the asteroid Castalia, mapped the stable region around this body, using numerical integrations for a gravitational field of a uniformly rotating prolate body. For this, Hu & Scheeres (2004) modelled Castalia using a triaxial ellipsoid. Furthermore, they demonstrated that resonances between a rotating body and the mean orbital

★ E-mail: tais.a.ribeiro@unesp.br

motion can play an important role in determining the stability of orbits.

In Olsen (2006), Castalia is used again as a target object for the study of stable regions around it, analysing prograde orbits with an inclination of 60° and retrograde orbits with an inclination of 150°. In the same work, the region around Itokawa is explored because it is an asteroid with slower rotation, compared to Castalia. In addition to the numerical experiments, Olsen (2006) derives analytical expressions for the widths of the mean motion resonances in gravitational fields of a uniformly rotating prolate body. The comparison made between the two models, analytical and numerical, points to a disagreement between theory and experiment for distances close to the asteroids that were objects of study. In Mysen, Olsen & Aksnes (2006) and Mysen & Aksnes (2007), a similar approach to the work studied in Olsen (2006) is performed for the comet 67P/Churyumov-Gerasimenko, modelling the body as a triaxial ellipsoid and mapping the unstable and stable zones.

In this work, the second in a series of articles that study Non-Spherical Symmetric Bodies (Madeira et al. 2022), we also seek to map the region around ellipsoidal bodies using the Poincaré surface of section technique. One of the target bodies of this work is the dwarf planet Haumea, which, because it is quite elongated and has a ring of particles, has become the object of study in several works in recent years. Ortiz et al. (2017) suggests that the ring is at the location of the 1:3 resonance between the orbital period of the ring particles and the spin of Haumea. However, Winter, Borderes-Motta & Ribeiro (2019) using the Poincaré surfaces of sections technique, shows that the orbits of this resonance have high eccentricities, above the limiting eccentricity to maintain the estimated ring width, concluding that the Haumea ring is not in resonance with the spin of the central body and the rings are possibly associated with the first kind orbits. They also show that the 1:3 resonance is double (2:6), generating a large region of chaos in the resonance separatrix. In addition, they mapped the stable zone of this resonance and the first kind orbits close to the ring.

We also mapped the region around the centaur 10 199 Chariklo, which has a system with two narrow rings and possibly small satellites (Braga-Ribas et al. 2014; Bérard et al. 2017). Sicardy et al. (2019) discusses the possibility that the centaur is spherical and has an anomalous mass at its equator. Other studies, based on observational data, suggest that Chariklo has a triaxial or Jacobi ellipsoid shape (Leiva et al. 2017; Morgado et al. 2021). In this work, we model Chariklo as an ellipsoid using the most recent observational data on its shape (Morgado et al. 2021).

In addition to Chariklo and Haumea, we map the stable and unstable regions of five other systems. These systems are hypothetical bodies in which we maintain part of the physical parameters of Haumea, but vary its ellipticity and period of rotation, to analyse the impact of these changes on the extensions of the stable and unstable regions.

The dynamic system adopted and the Poincaré surface of section technique are considered in the next section. The dynamic characteristics of some of the controlled orbits found in this study are explored in Section 3. Maps of stable and unstable regions are presented and discussed in Section 4. The applications of this study are explored in Section 5 and finally, we present our conclusions in Section 6.

2 DYNAMICAL SYSTEM

In this work, we analyse the dynamics of particles around prolate bodies in the rotating system (Fig. 1). Observational data from the

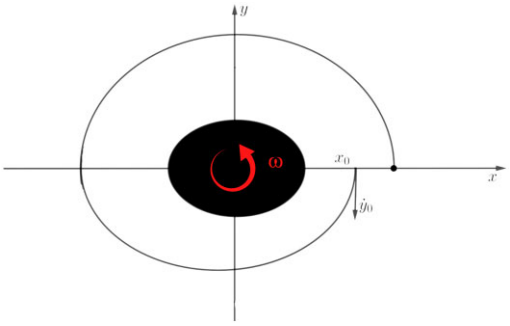

Figure 1. Schematic diagram of an equatorial path around a Jacobi ellipsoid. The plane Oxy is fixed on the body, x_0 marks the initial position of the trajectory and the arrow indicates the initial velocity.

works of Ortiz et al. (2017); Morgado et al. (2021) suggests the Jacobi ellipsoid as a possible shape for the bodies chosen as the target of this study. Therefore, the gravitational potential of these bodies will be composed by the spherical harmonics J_2 and C_{22} defined as (Balmino 1994):

$$J_2 = -\frac{2C^2 - A^2 - B^2}{10R_e^2}, \tag{1}$$

and

$$C_{22} = \frac{A^2 - B^2}{20R_e^2}. \tag{2}$$

We take $R_e = (ABC)^{1/3}$ as the equivalent radius.

The equations of motion, with a plane Oxy fixed on the central body and rotating with the same period of rotation as the central body, as illustrated in Fig. 1, are given by (Hu & Scheeres 2004):

$$\ddot{x} - 2\omega\dot{y} = \omega^2 x + U_x, \tag{3}$$

and

$$\ddot{y} + 2\omega\dot{x} = \omega^2 y + U_y, \tag{4}$$

where ω is the velocity of rotation of the central body, U_x and U_y are the derivatives of the gravitational potential defined as:

$$U(x, y) = \frac{GM}{r}\left(1 - \left(\frac{R_e}{r}\right)^2\left[\frac{-J_2}{2} - \frac{3C_{22}}{r^2}\left(x^2 - y^2\right)\right]\right), \tag{5}$$

where $r = \sqrt{x^2 + y^2}$, G is the gravitational constant and M is the mass of the central body.

The systems explored have the Jacobi constant C_j that can be given by (Hu & Scheeres 2004):

$$C_j = \omega^2\left(x^2 + y^2\right) + 2U(x, y) - \dot{x}^2 - \dot{y}^2, \tag{6}$$

which will be used to obtain the Poincaré surface of section. The unit of Jacobi's constant is km^2s^{-2}, however, for practicality, we will omit this information in the figures presented in this work. In the following subsections, we explore the Poincaré surface of section technique and some of the families of periodic orbits found in the systems studied in this work.

2.1 Poincaré surface of section

Poincaré surface of section are maps generated by crossing points of the trajectories in the phase space with a fixed section of the system. These maps are generated in phase space for fixed values of the Jacobi constant (equation 6). This technique has been used extensively in

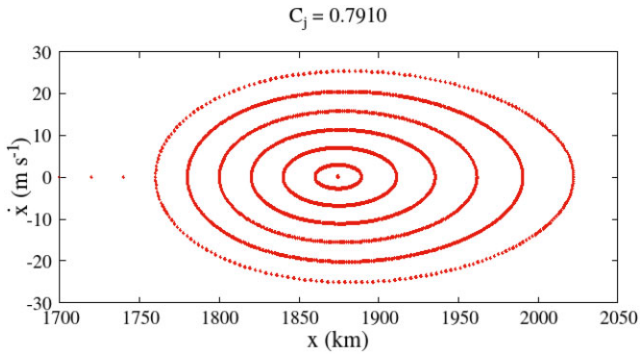

Figure 2. Poincaré surface of section for a system considering Haumea as an oblate body, i.e. the ellipticity coefficient (C_{22}) is equal to zero. The islands in red are quasi-periodic orbits associated with a family of periodic orbits, indicated by the single point at the centre of all the islands.

celestial dynamics as a tool for identifying the location and extent of stable and unstable regions in the circular restricted three-body problem (Hénon 1965a, b, 1966a, b, 1969; Jefferys 1971; Winter & Murray 1994a, b, 1997a, b). However, in recent years, Poincaré surface of section has been applied to the two-body problem, whose central body rotates and has a non-spherical mass distribution (Borderes-Motta & Winter 2018; Winter et al. 2019; Madeira et al. 2022). Fig. 2 shows a Poincaré surface of section applied to the two-body problem whose central object is oblate. The primary body has the same physical parameters as Haumea (these parameters can be seen in Table 1) but with the coefficient C_{22} equals to zero. In this case, when there is no ellipticity, we only have elliptical orbits, indicated by the red curves, a circular orbit, represented by the point in the centre of the red curves, and hyperbolic trajectories that collide with the central body or are ejected, indicated by isolated red points.

In cases where the body is prolate, the ellipticity of the body together with its rotation are responsible for disturbing the region and generating more complex structures, related to resonances between the rotation of the primary and the orbital motion of the particles, as can be seen in the Fig. 3, which shows two Poincaré surfaces of sections of the Haumea system. The physical parameters used can be consulted in Table 1. First, a few dozen initial conditions were distributed for distances $2000 < x < 2300$ km and $\dot{x} = 0$ ms^{-1}. Through a set of numerical integration, the Poincaré surface of sections are generated. The points randomly distributed correspond to chaotic orbits and determine the dynamically unstable regions. The stable regions are delimited by points that form closed curves, which do not cross each other. These curves are called islands of stability. Random points from chaotic orbits do not enter these stable regions. Each island of stability is formed by a quasi-periodic orbit, which receives this nomenclature because it does not have a defined orbital period. However, these quasi-periodic orbits follow the behaviour of the periodic orbits that are located in the centre of stability islands.

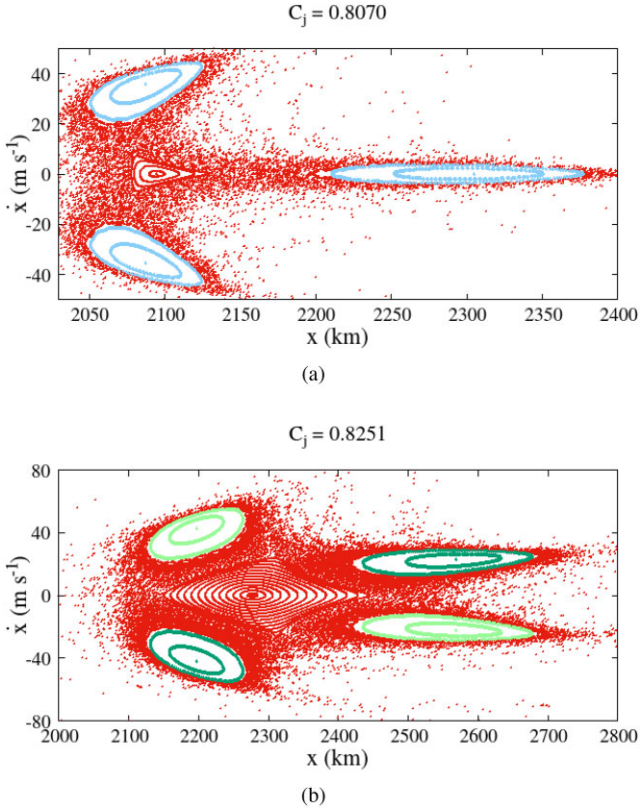

Figure 3. Poincaré surface of section for two different values of the Jacobi constant (C_j). The stability islands of the 2:5 resonance are shown at the top, indicated by the blue colour, while the double stability islands of the 2:6 resonance are shown in the bottom figure, represented by different shades of green. On both Poincaré surfaces of sections, there is the presence of islands of quasi-periodic orbits associated with periodic orbits of the first kind (closed red curves), in addition to the unstable region, filled randomly by red points.

Periodic orbits, whenever they cross the Poincaré surface of section, pass through the same points in the phase space.

The periodic orbits present in Fig. 3 can be classified, according to Poincaré (1895), as first or second kinds. The first kind is quasi-circular orbits that are not associated with any resonance. Fig. 3 are the points in the centres of the islands of stability represented by the red colour. The second kind are the periodic orbits associated with resonances. In this case, spin-orbit resonances, i.e. resonances between the rotation of the primary body and the orbital motion of the secondary body. Periodic orbits of the first kind are identified by single islands of stability in the Poincaré surface of section, while those of the second kind can be identified by unit islands, pairs, or an integer number of islands of stability. This number is equal to the order of the resonance. For example, in Fig. 3(a) there are three blue islands, therefore it is a third-order resonance associated with 2:5

Table 1. Physical parameters of central bodies used in the numerical simulations.

System	Chariklo	Haumea	Haumea[a]	Haumea[b]	Haumea[c]	Haumea[d]	Haumea[e]
Mass (kg)[1, 2]	6.432×10^{18}	4.006×10^{21}	4.006×10^{21}	4.006×10^{21}	4.006×10^{21}	4.006×10^{21}	4.006×10^{21}
Equivalent radius (km)	124.8	798	798	798	798	798	798
Spin (h)[1, 3]	7.004	3.9155	3.9155	3.9155	3.9155	11.7465	19.5775
J_2	0.124	0.243	0.243	0.243	0.243	0.243	0.243
C_{22}	0.007	0.049	0.034	0.018	0.003	0.049	0.049

Note.[1] Leiva et al. (2017). [2]Ragozzine & Brown (2009). [3]Rabinowitz et al. (2006).

resonance. These islands of stability related to the same resonance or the first kind periodic orbits, occur along an interval of C_j values, varying their location and size. This set of periodic orbits is called a family.

Fig. 3(b) shows two pairs of stability islands in light green and dark green. These are two families belonging to the same resonance. Duplicity in families is a natural feature due to the potential of the body being invariant under a rotation π (Sicardy 2020) and it occurs for all 1:n. Because of that, following Sicardy (2020), we will call them 2:2n resonance. Thus, the two families in Fig. 3(b) are associated with the 2:6 resonance.

2.2 Other periodic orbits

There are periodic orbits that do not fit the first and second kinds classifications but also delimit regions of stability. Broucke (1968) mapped and classified several of these orbits in the Earth–Moon system and Winter & Neto (2002) investigated the stability zones delimited by them, in the same Earth–Moon system. In this work, we found two families of these periodic orbits in the system composed of a central body with the same physical parameters as Haumea, but with three times the rotation period of the dwarf planet (see data in Table 1, case Haumea^d). Fig. 4 presents the evolution of the two families (in shades of blue) for four Jacobi constant values. Due to the shape of the trajectory these two families fit into the F-type classification, defined in the work of Broucke (1968). For simplicity, they will be called F1 and F2. Furthermore, the periodic orbits of these two families are symmetric trajectories and with a large radial variation.

These two families delimit regions of stability that will be discussed in Section 4. Next, we present the evolution of the families associated with resonances of up to the third order.

2.3 Resonances

In this work, we use the Poincaré surface of section technique to determine stable and unstable regions around prolate bodies. Part of the stable region found is due to the presence of resonances. We will analyse the resonances of up to the third order, which is the strongest presence in the systems considered in this work. To demonstrate the evolution of these resonance families in the phase space, we show in this section some of the Poincaré surfaces of sections for four cases of the central body of the system: the dwarf planet Haumea; the hypothetical Haumea^c body, which has the same physical parameters as Haumea, except for the ellipticity, with a minimum value for the Poincaré surface of section to appear resonant structures; and the hypothetical system Haumea^e, which has a rotation period five times slower than that of Haumea. In addition to these four cases, the study extends to three more hypothetical central bodies, which are variations of the rotation period and ellipticity coefficient of Haumea and to the Chariklo system case. The variation of these two parameters was made to analyse its implications in the stability regions of the systems. The physical parameters used in the numerical simulations for each system are shown in Table 1.

Fig. 5 presents a sequence of the Poincaré surface of section for six values of the Jacobi constant, allowing the visualization of the evolution of the structures of the first and second kinds periodic/quasi-periodic orbits. Three resonances are highlighted: 2:4 ((a) and (b)), 2:5 ((c) and (d)) and 2:4 ((e) and (f)). The 2:4 resonance is double, represented by the pink and purple islands in Figs 5(a) and (b). For the first Jacobi constant value, there are no periodic/quasi-periodic orbits of the first kind, as the entire region is chaotic, as indicated by the

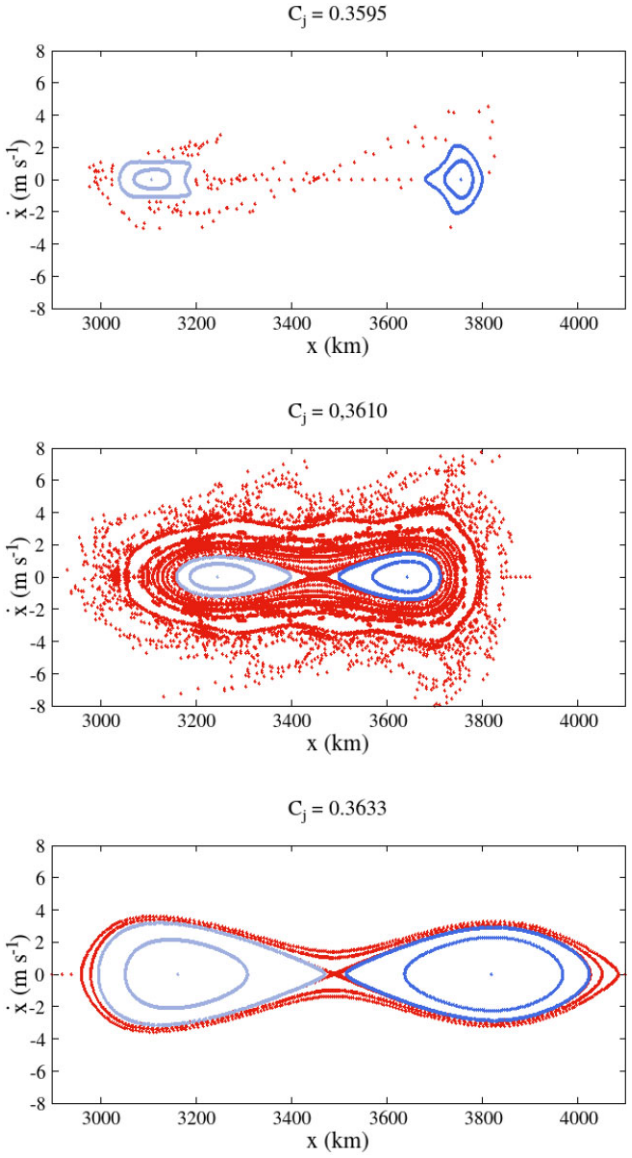

Figure 4. Poincaré surface of section of the Haumea^d system (see Table 1) for four different values of the Jacobi constant (C_j), showing the evolution of two families, of periodic and quasi-periodic orbits, indicated by the colours light blue (F1) and dark blue (F2).

random red points that fill the region around the islands of stability of the 2:4 resonance. This is due to the proximity to the central body, the particles collide or are ejected. In Fig. 5(b) the existence of the chaotic region can still be seen, but there is a region of stability associated with quasi-periodic orbits of the first kind, closed red curves. The islands of stability associated with the 2:4 resonance are closer and smaller, a natural motion when the Jacobi constant is increased. Due to this approximation, a separatrix appears between the islands, generating a narrow region of chaos. The chaos between the islands destroys the periodic orbit of the first kind. Therefore, for the Jacobi constant interval, in which it is possible to identify the existence of the 2:4 resonance, the first kind of periodic orbit does not exist.

Fig. 5(c) shows the stability islands associated with the 2:5 resonance, in blue. There is a small region with periodic/quasi-periodic orbits of the first kind and, around it, a large region of

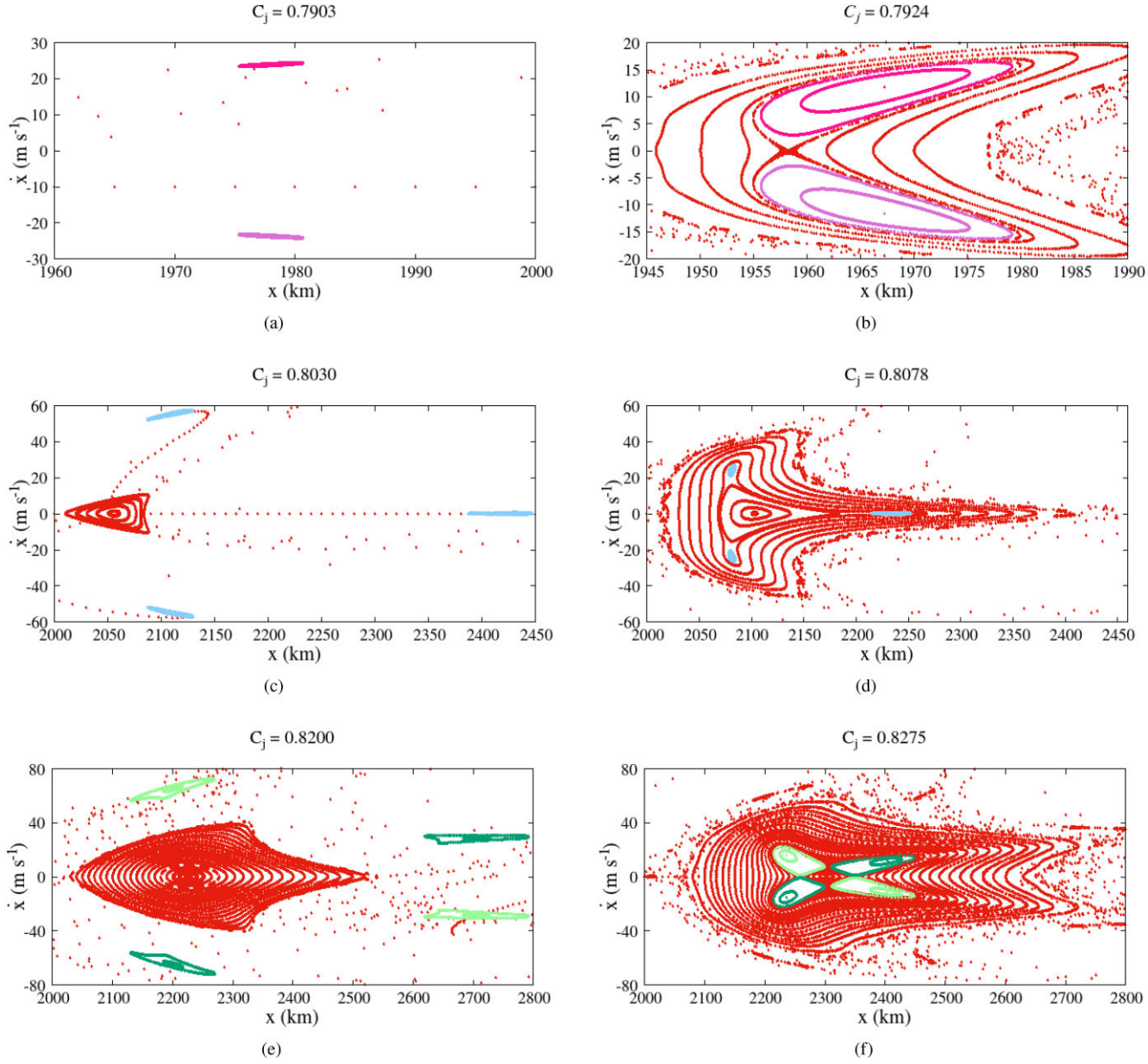

Figure 5. Poincaré surfaces of sections of the Haumea system for six different values of the Jacobi constant (C_j), showing the evolution of the 2:4, 2:5, and 2:6 resonances. The stability islands of the 2:4 resonance (plots (a) and (b)) are duplicated and are represented by pink and purple colours. The same phenomenon occurs with the islands of the 2:6 resonance (plots (e) and (f)), indicated by different shades of green. The 2:5 resonance is shown by the islands in blue in plots (c) and (d). The islands in red are quasi-periodic orbits associated with a family of periodic orbits of the first kind.

chaos. In the following plot, 5(d), it can be seen that the islands of the 2:5 resonance are closer and smaller, however, in this case, these islands do not continue to approach the centre of the first kind periodic orbits. This is the closest approximation between them and for larger values of C_j, these islands are no longer identified in the Poincaré surface of section.

Changing on to the Poincaré surface of section where the two families of the 2:6 resonance appears, Figs 5(e) and (f), there is a considerable increase in the stable region, both limited by first kind and resonance orbits. This fact is explained by the distance from the central body, reducing the perturbation due to ellipticity in the gravitational field.

Fig. 6 shows a set of Poincaré surface of section for the Haumea^c system, which has the ellipticity coefficient lower than the real Haumea value of C_{22}. This is the smallest value of C_{22} that generates structures related to spin-orbit resonances, for this system. The first observable change is the displacement of the structures on the x axis: they are closer to the central body. Note that, in general, the unstable region is smaller, identified by the random red points. The family of periodic orbits of the first kind still does not coexist with the families of the 2:4 resonance. In Fig. 6(b), the points that follow a curve in the region between $1765 < x < 1770$ km for $\dot{x} < 0$ m s^{-1} and $1783 < x < 1790$ km for $\dot{x} > 0$ m s^{-1} are orbits that initially have the motion of quasi-periodic orbits, but collide with the central body after some period of time. The collision occurs because the proximity to the central body increases the probability of more eccentric trajectories colliding with the primary. The same phenomenon occurs in Figs 6(b) and (c).

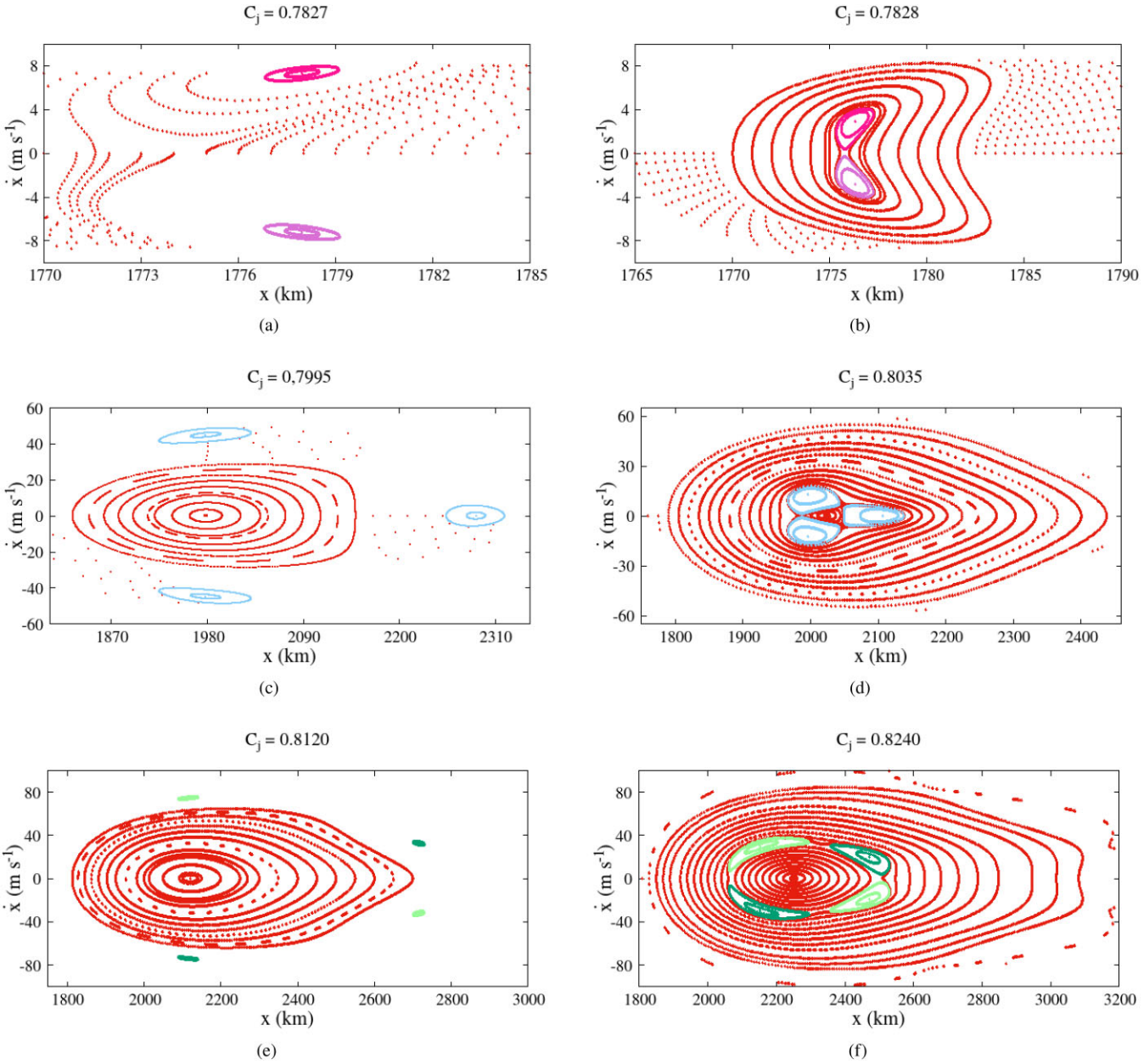

Figure 6. Poincaré surface of section of the Haumea^c system for six different values of the Jacobi constant (C_j), showing the evolution of the 2:4, 2:5 and 2:6 resonances. The stability islands of the 2:4 resonance (plots (a) and (b)) are duplicated and are represented by pink and purple colors. The same phenomenon occurs with the islands of the 2:6 resonance (plots (e) and (f)), indicated by different shades of green. The 2:5 resonance is shown by the islands in blue in plots (c) and (d). The islands in red are quasi-periodic orbits associated with a family of periodic orbits of the first kind.

Haumea's high spin, added to its elongated shape, causes for those particles orbiting close to it to collide or to be ejected from the system. Decreasing the rotation, all the resonant semimajor axes move away from the central body, allowing other resonances to appear, for example, the 4:7 resonance represented by the yellow islands in Fig. 7 present in the Haumea^e system. Also, on this system occurs the bifurcation of the 2:6 resonance, which can be seen in Fig. 8(a) by the dark and light green points. Previously, each periodic orbit associated with the 2:6 resonance crossed the phase space at only two points, but due to the bifurcation, it now crosses at four different points. Figs 8(b) and (c) shows the zoom of the bifurcated islands of one of the families associated with the 2:6 resonance. Around them, there is a region of chaos intrinsic to the separatrix, generated by the bifurcation, restricting the extension of the stable region of the resonance, compared to cases in which there is no bifurcation. This phenomenon entails some implications, such as the radial extension of a possible ring around this body in 2:6 spin-orbit resonance: the chaos generated by the separatrix would produce a gap inside the ring. The evolution of these families in phase space can be seen in Fig. 9.

3 PERIODIC ORBITS AROUND PROLATE BODIES

The orbits associated with the resonances discussed in Section 2.3 are studied here in order to discuss their dynamical characteristics. For

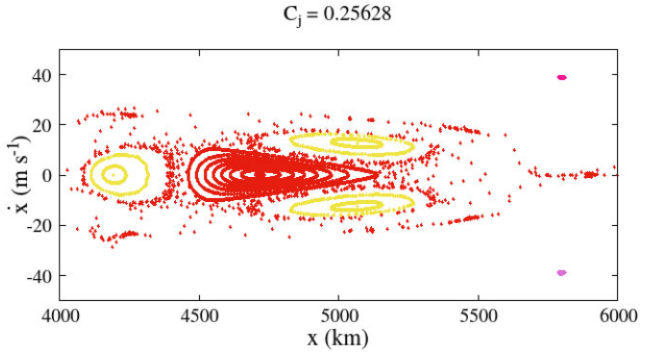

Figure 7. Poincaré surface of section of the Haumea^e. The 4:7 resonance is represented by the islands in yellow. The islands in red are quasi-periodic orbits associated with a family of periodic orbits of the first kind. The islands in pink and lilac belong to the 2:4 resonance.

this, we choose a periodic orbit for each resonance of the Haumea system and a periodic orbit of the 4:7 resonance of the Haumea^e system. It is noteworthy that the behaviour of the resonant orbits of the other analysed systems are similar to the one presented in this section. As said, the 2:4 resonance has two families of periodic/quasi-periodic orbits, so in Fig. 10 a pair of these periodic orbits are presented for $C_j = 0.7903$ km^2 s^{-2}, one from each family. Fig. 10(a) refers to the periodic orbit represented by the central point interior to the pink islands of the Poincaré surface of section and Fig. 10(b) refers to the purple periodic orbit, both shown in Fig. 5(a). The trajectories are in the rotating system and are retrograde. The orbit is closed because the particle is at the fixed point of the resonance. The temporal evolution is given by the numbered points that are equally spaced in time, while the scale and colours give the velocity in the inertial system. The points closest to the central body have the highest velocity modules, indicating the pericentre of the orbit. Likewise, the lowest values of velocities indicate the region of the apocentre of the orbit. The trajectories are mirror images of each other about the line Oy. These are consequences that result from the gravitational potential being invariant under a rotation π (equation 5). The period of these orbits corresponds to two periods of rotation of Haumea.

Fig. 11 shows the periodic orbit, in the rotating system, associated with the 2:5 resonance for a $C_j = 0.8030$ km^{2}s^{-2}. This orbit is represented by the central point interior to the blue islands of stability in Fig. 5(c). In this case, the orbit is symmetrical in both axes, the Ox axis and the Oy axis. The period of this orbit is approximately five times the period of rotation of Haumea and it is a closed trajectory because it is at the resonance fixed point.

As it happens for the 2:4 resonance, there is a duplicity of families of periodic/quasi-periodic orbits in the 2:6 resonance, as seen in the Poincaré surface of section in subsection 2.3. Fig. 12 presents a sample of these periodic orbits for the value of $C_j = 0.8200$ km^{2}s^{-2}. In Fig. 12(a), there is the trajectory of the central point interior to the light green islands of the Poincaré surface of section and Fig. 12(b) shows the central point interior to the islands in dark green colour, both shown in Fig. 5(e). The orbital period is three times the rotational period of Haumea. As it is a double family belonging to the same resonance, the orbits are mirror images of each other about the Ox axis. In the Oy axis, there is a division of the orbits into symmetrical parts, due to the symmetry of the body to the same aforementioned axis. The closest points of the trajectory with the central body are the same where the velocity module assumes the highest values, indicating the pericentre locations. At

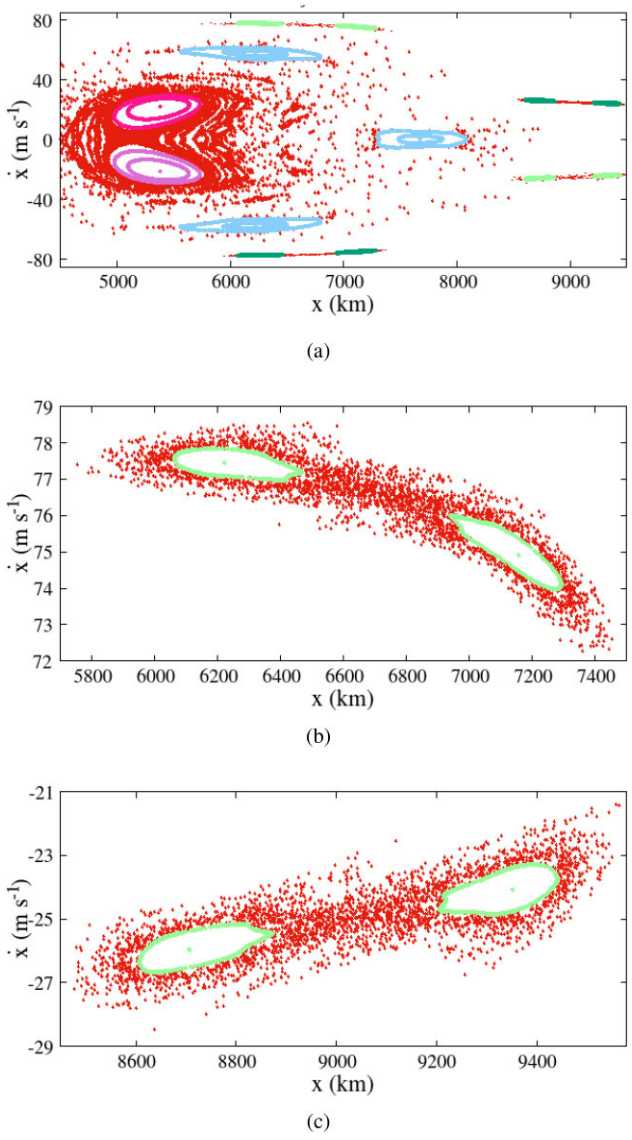

Figure 8. Poincaré surface of section of the Haumea^e system for $C_j = 2.6115 \times 10^{-1}$ km^{2}s^{-2}. (a) The stability islands of the 2:4 resonance are duplicated and are represented by pink and purple colours, the same phenomenon occurs with the islands of the 2:6 resonance indicated by different shades of green, the 2:5 resonance is shown by the islands in blue and the islands in red are quasi-periodic orbits associated with a family of periodic orbits of the first kind. (b) and (c) zoom of the bifurcation of one of the families associated with 2:6 resonance.

the points of closest approximation to Haumea, the velocities are lower, corresponding to the apocentres.

Fig. 13 shows the periodic orbit, in the rotating system, associated with the 4:7 resonance of the Haumea^e system for a $C_j = 0.25536$ km^{2}s^{-2}. This orbit is represented by the central point interior to the yellow stability islands in Fig. 7. Because it is not a double resonance, the orbit is symmetrical in both axes, the Ox axis and the Oy axis. The period of this orbit is seven times the period of rotation of Haumea.

The plots in Fig. 14 show the temporal evolution of the radial distance of the periodic orbits associated with the (i) 2:4, (ii) 2:5, (iii) 2:6, and (iv) 4:7 resonances. Figs 14(a) and (c) refer to the families that were represented by pink and light green colours, in the

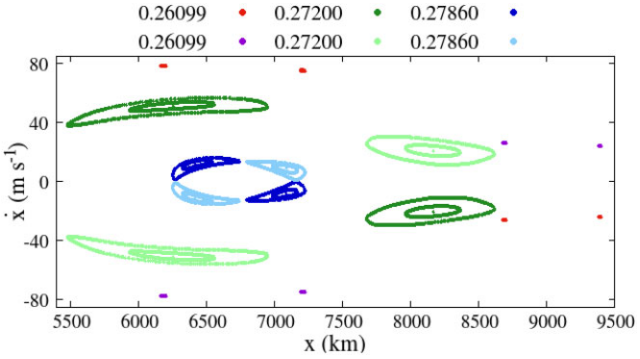

Figure 9. Evolution of the families associated with the 2:6 resonance in the Poincaré surface of section for the Haumea^e system. The plot presents a sample of the largest islands of stability, an intermediate island, and the internal points that represent the periodic orbit, showing the structure for different values of C_j. The colours indicate the values of C_j.

Poincaré surface of section of Fig. 5. The colours of the solid lines indicate distinct values of the Jacobi constant. The orbits with the highest radial amplitudes (yellow) correspond to the lowest values of C_j, while the trajectories with the lowest radial amplitude (solid grey lines) correspond to the highest values of C_j. The intervals of the considered Jacobi constants can be seen in the captions of each plot present in Fig. 14. The comparison between the orbits of the same family for different C_j shows that the greater the value of C_j, the smaller is the amplitude of the radial variation. This attenuation occurs as the islands of stability approach the first kind orbit in the Poincaré surface of section. The dotted and dashed lines delimit the location of the resonant semimajor axis using two different methods: through the epicyclic frequencies (Borderies & Longaretti 1987; Longaretti & Borderies 1991; Borderies & Longaretti 1994) and the geometry of the orbit. The η and κ frequencies are defined as (Sicardy 2020):

$$\eta^2 = \frac{GM}{a^3}\left[1 + \frac{3f}{5}\left(\frac{R}{a}\right)^2\right] \tag{7}$$

and

$$\kappa^2 = \frac{GM}{a^3}\left[1 - \frac{3f}{5}\left(\frac{R}{a}\right)^2\right], \tag{8}$$

where $f = 2.5\ J_2$. The resonant semimajor axis, a, is obtained by a numerical iteration process using the two frequencies (for more details see Renner & Sicardy 2006). The values presented in the graphs of Fig. 14 (dotted lines) using this method are the same values obtained in Sicardy (2020).

The second method for finding the resonant semimajor axis is derived from the geometry of the orbit. This method was discussed in Ribeiro et al. (2021), which consists of calculating the semimajor axis using the equation:

$$a = \frac{r_{\max} + r_{\min}}{2}, \tag{9}$$

where a is the semimajor axis due to the geometry of the orbit, $r_{\max}$ and $r_{\min}$ are the largest and smallest radial distances of the same orbit, respectively. The diagram in Fig. 15 shows an overview of the comparison between the three methods used to locate the centres of resonances and the radial width of the resonant orbits. The diagram is divided into three horizontal bands. Each track refers to one resonance. The grey regions limit the width of the orbital radius variation of the trajectories indicated by the grey colours in Fig. 14.

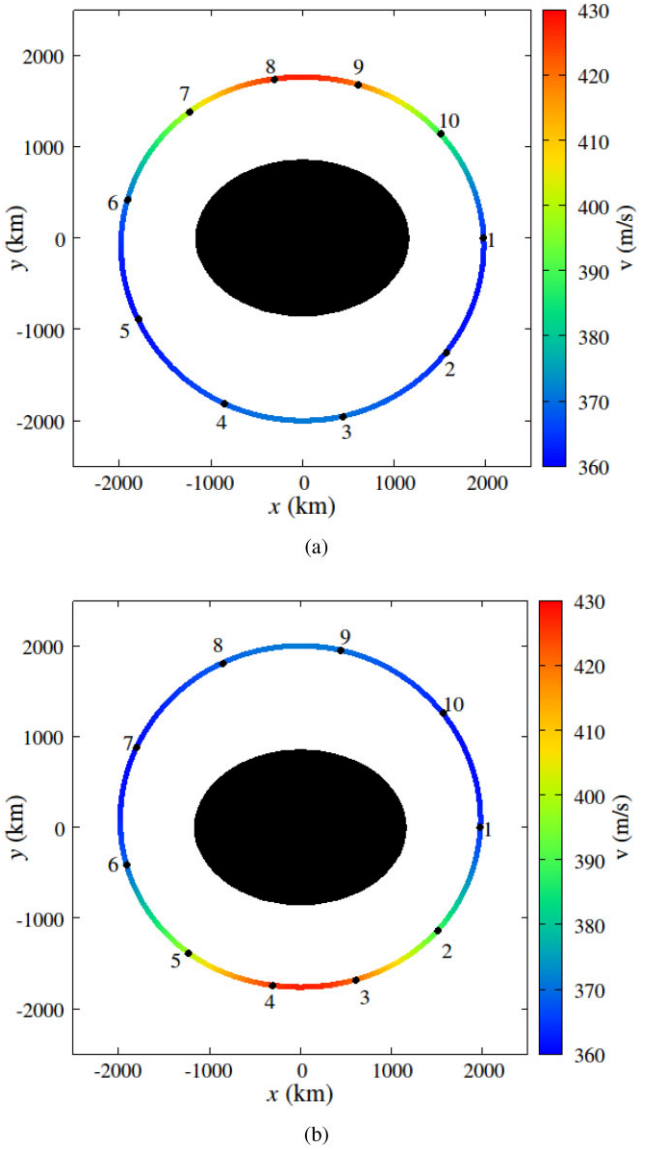

Figure 10. Periodic orbits of the 2:4 resonance for $C_j = 0.7903$ km^2 s^{-2} in the rotating system. The temporal evolution of the orbits is given by the numbered points that are equally spaced in time, while the colour scale gives the velocity in the inertial system. (a) The periodic orbit of the family represented by the pink colour in Fig. 5(a). (b) The periodic orbit of the family represented by the purple colour in Fig. 5(a).

These are the periodic orbits with smaller amplitudes of the radial variation. Among the three orbits analysed, the one associated with 2:5 resonance is the one with the greatest extent of radial variation, around $\Delta r = 307$ km, while the orbit associated with 2:4 resonance has $\Delta r = 83$ km and at 2:6 has $\Delta r = 118$ km. The radial extent of the 2:5 resonance orbits is larger because its family is not double, as well as the 2:4 and 2:6 resonances.

As explored in Ribeiro et al. (2021), there is a difficulty in describing, in terms of orbital elements, trajectories around prolate bodies. The diagram in Fig. 15 highlights this difficulty. In the 2:4 resonance range the location of the resonant semimajor axis calculated using the two-body problem (pink dotted line), which considers the central body to be spherical, is outside the radial width of the orbit and distant about 133 km from the $r_{\min}$ of this orbit. The same occurs with the resonant semimajor axis obtained

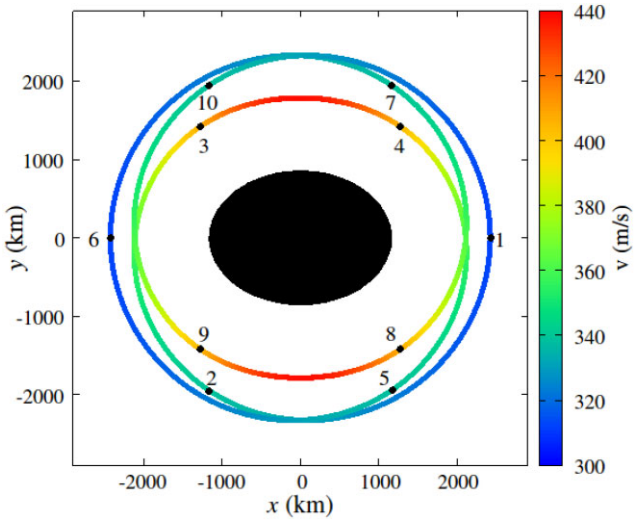

Figure 11. Periodic orbit of the 2:5 resonance for $C_j = 0.8030$ km^2 s^{-2} in the rotating system. The temporal evolution of the orbit is given by the numbered points that are equally spaced in time, while the colour scale gives the velocity in the inertial system.

through the epicyclic frequencies (pink dot-dash line), which only considers the perturbation of the oblateness of the body. Going back to Fig. 14(a), note that the 2:4 resonant semimajor axis obtained by the epicyclic frequencies is outside the region of the orbit with the greatest amplitude of radial variation (yellow line). Both method do not take into account the perturbation due to the ellipticity of the central body.

Because they are farther from the primary body, particles at the 2:5 resonance are less affected by the effect of the ellipticity of the body, compared to the particles at the 2:4 resonance. For this reason, the difference between the resonant semimajor axis calculated by the two mentioned methods is closer to the centre of the radial band of the orbit. However, this difference, around 69 km, is still considerable. For the 2:6 resonant orbit, the difference does not reach 2 km. Because the theoretical models are not accurate to determine the resonant semimajor axis, especially those closer to the central body, to use the orbit geometry method becomes an alternative. The dashed lines in the diagram of Fig. 15 indicate the semi-axis of each of the resonances making use of the geometry of the orbit of smaller radial amplitude (solid grey lines). In the following section, the stable and unstable regions around prolate bodies are identified using this method.

4 WIDTH OF RESONANCES

Having defined the method that best fits the calculation of the resonant semimajor axis, we extend this application to determine the width of resonances and the limits of the stable and unstable regions around bodies with ellipticity. Fig. 16 shows how the resonance width is determined for a given value of C_j. In Fig. 16, we have the temporal evolution of the radial variation of the periodic (pink line) and quasi-periodic (yellow line) orbits associated with the 2:4 resonance. The quasi-periodic orbit chosen is always the largest island of stability found in the Poincaré surface of section, as this guarantees the maximum width of the resonance. With the periodic orbit, the centre of resonance is determined, while with the quasi-periodic orbit, the limits of the width of the resonance can be obtained. To determine the lower limit, the equation $a = (r_{\min} + r_{\max})/2$ is used again, where the values of the maximum and minimum radii are those indicated by the

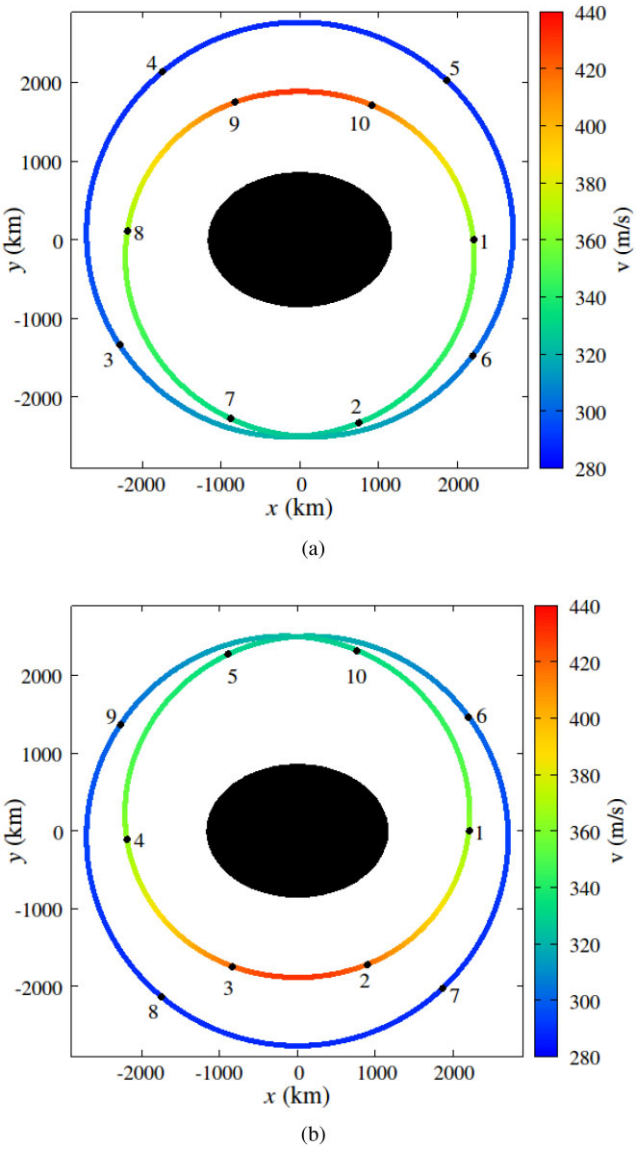

Figure 12. Periodic orbits of the 2:6 resonance for $C_j = 0.8200$ km^2 s^{-2} in the rotating system. The temporal evolution of the orbits is given by the numbered points that are equally spaced in time, while the colour scale gives the velocity in the inertial system. (a) The periodic orbit of the family represented by the light green colour in Fig. 5. (b) The periodic orbit of the family is represented by the dark green colour in Fig. 5.

dashed lines and yellow arrows, which is the smallest difference of the radial variation. For the upper width limit, use the radius values of the greatest radial variation, indicated by the dashed lines and grey arrows. This process is done for all orbits of the 4:7, 2:4, 2:5, 2:6 resonances and for orbits of the first kind family. In addition to calculating the semimajor axis due to geometry, its respective eccentricities are also calculated by the equation $e = 1 - r_{\min}/a$. With these data, it is possible to build the map of the unstable and stable regions in the $a - e$ space. This process was done for all the seven systems addressed in this work.

Fig. 17 shows the mapping of the region around the Haumea systems, Haumea,[a] Haumea[b] and Haumea[c]. Starting with the Haumea system, Fig. 17(a), since it is a very elongated body, the region of stability due to the family of the first kind orbits (white region limited by red lines), is greatly affected by the unstable region (in grey). This

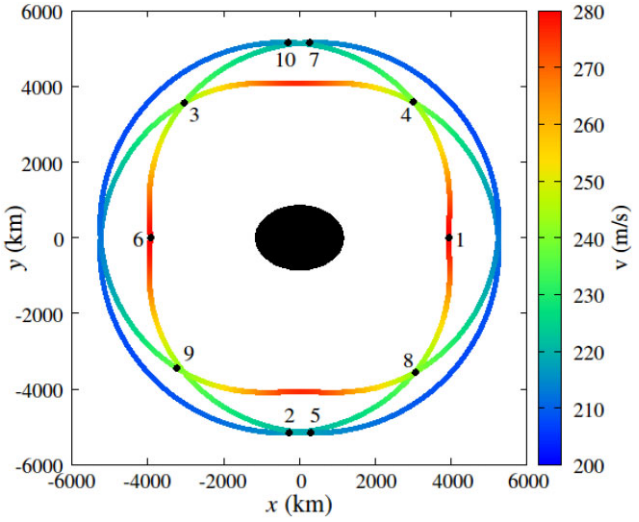

Figure 13. Periodic orbit of the 4:7 resonance of the Haumea^e system for $C_j = 0.25536$ km^2 s^{-2} in the rotating system. The temporal evolution of the orbit is given by the numbered points that are equally spaced in time, while the colour scale gives the velocity in the inertial system.

phenomenon can also be noticed by analysing the Poincaré surface of section, Fig. 5, with the presence of regions of chaos, indicated by the red points randomly filling the spaces. The pink, blue, and green regions correspond to the widths of the 2:4, 2:5, and 2:6 resonances, respectively. Of the three, the largest in semimajor axis length and eccentricity is the 2:6 resonance. Due to the proximity to the central body, the width of the 2:4 resonance is considerably small. As seen in the Poincaré surface of section, this resonance is surrounded by a large region of chaos. It is observed that for low values of the eccentricity, $e < 0.018$, there are no regions of stability associated with any of the three considered resonances. However, the periodic orbits of the first kind, represented by the lower red line, always remain with an eccentricity below 0.02.

Observing the maps of the Haumea^a and Haumea^b systems, see Figs 17(b) and (c), it is noted that the stable region due to the first kind orbits is greater as the ellipticity of the body decreases. Furthermore, the eccentricity of periodic orbits of the first kind is also closer to zero. Fig. 17(d) shows the mapping of regions around the Haumea^c system, which has the lowest ellipticity coefficient of the systems considered in this work. For this case, the coefficient C_{22} was minimized to 0.003, which is the smallest value sufficient to generate more complex structures, involving resonances between the Haumea rotation and the orbital motion of the particles. With the perturbation of the reduced ellipticity of the body, the stable region becomes larger and the upper red line has a smooth grow, different from what is shown in Fig. 17(a), where there are sharp drops on the eccentricity of quasi-periodic orbits of the first kind. The lower red line, which is related to periodic orbits of the first kind, shows that the eccentricity is approximately zero. As for the widths of the resonances, for the case of the 2:4 resonance there was a considerable reduction in its size and the 2:5 and 2:6 resonances became less asymmetrical about their respective centres (dashed lines), consequences caused by the attenuation of the ellipticity of the central body.

Fig. 18 shows the maps for the systems where only the rotation period has changed in relation to the physical data of Haumea. In general, in both cases, the regions of stability due to the resonances became wider in the semimajor axis and covered a wider range of eccentricity. This occurs because the rotation is slower, which

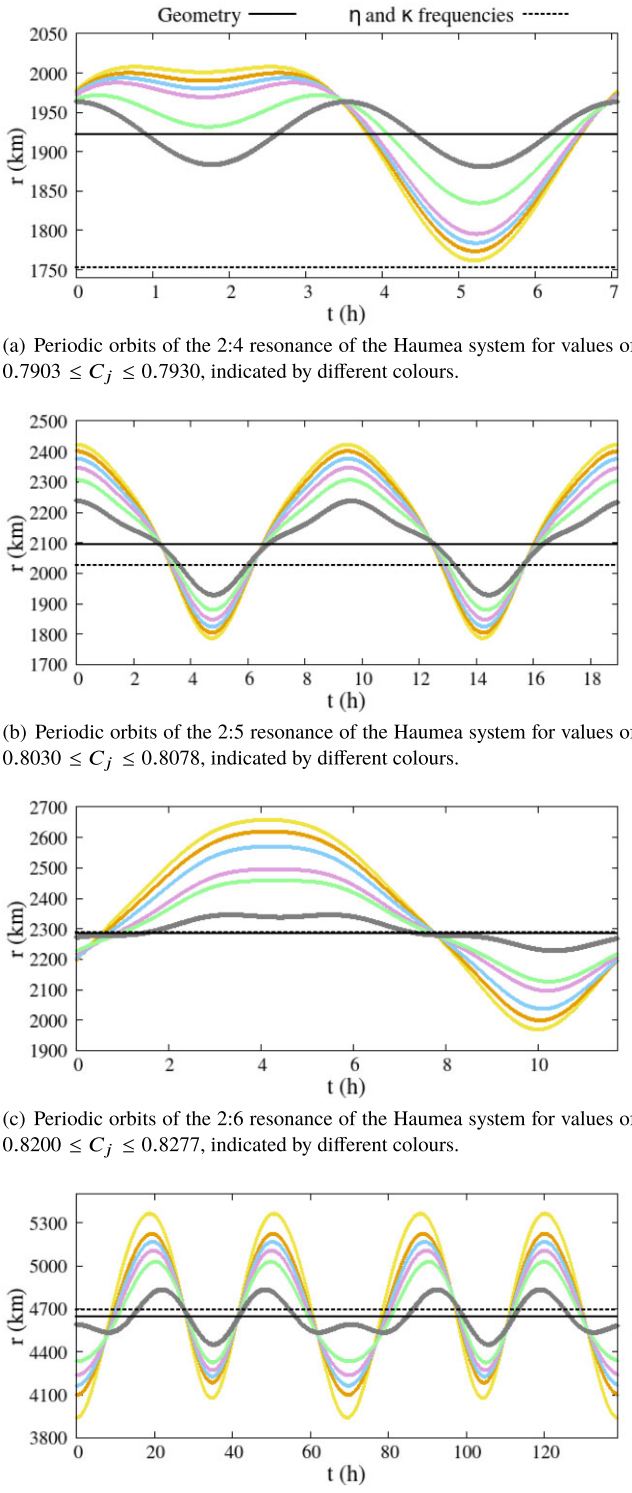

(a) Periodic orbits of the 2:4 resonance of the Haumea system for values of $0.7903 \leq C_j \leq 0.7930$, indicated by different colours.

(b) Periodic orbits of the 2:5 resonance of the Haumea system for values of $0.8030 \leq C_j \leq 0.8078$, indicated by different colours.

(c) Periodic orbits of the 2:6 resonance of the Haumea system for values of $0.8200 \leq C_j \leq 0.8277$, indicated by different colours.

(d) Periodic orbits of the 4:7 resonance of the Haumea^e system for values of $0.25536 \leq C_j \leq 0.25676$, indicated by different colours.

Figure 14. Temporal evolution of the radial distance of the periodic orbits associated with the resonances, for different values of C_j. Time refers to an orbital period in the rotating system. The dashed lines indicate the resonant semimajor axis location obtained from two different methods.

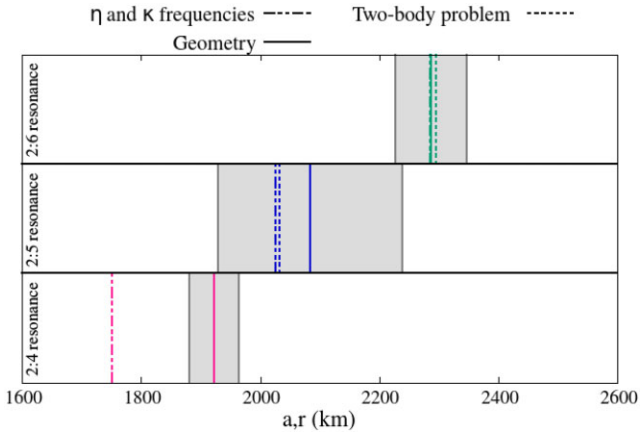

Figure 15. Diagram comparing the location of the semimajor axis of the 2:4, 2:5, and 2:6 resonances, calculated by three different methods: two-body problem, epicyclic frequencies (η and κ) and orbit geometry. The types of dashes indicate which method was used. The pink, blue, and green colours are related to the resonances and the grey regions indicate the radial variation of the less eccentric periodic orbit of each considered resonance. In the case of the 2:4 resonance, the locations of the resonant semimajor axis calculated through the two-body problem and epicyclic frequencies are very close, with the lines almost overlapping.

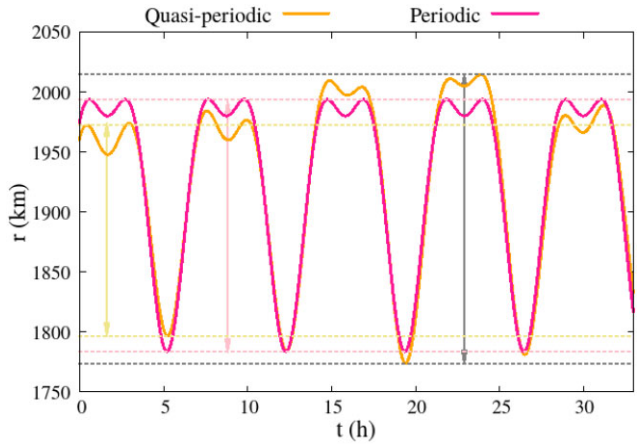

Figure 16. Temporal evolution of the radial variation of the periodic (in pink) and quasi-periodic (in yellow) orbits. The quasi-periodic orbit refers to the largest island associated with 2:4 resonance for the Jacobi constant $C_j = 0.7912$ km^{2}s^{-2}. The yellow and grey dashed lines and arrows indicate the maximum and minimum radial distance values used to calculate the semimajor axis and eccentricity limits of the quasi-periodic orbits, while the pink dashed lines and arrows point to the maximum and minimum values of the radial distance considered to calculate the centre of resonance.

leaves the resonances considered further away from the central body, minimizing collisions and ejections. In the Haumea^e system, see Fig. 18(b), in addition to the slower rotation period allowing the emergence of the 4:7 resonance, yellow region, one can note the segmentation of the stability region due to the orbits of the first kind. This segmentation is caused by the chaos of the separatrix of the 2:4 resonance. Unlike the other cases, in Haumea^e, the periodic orbits of the first kind have also higher eccentricities, starting at $e \approx 0.1$. In the stability region of the 2:6 resonance, Fig. 18(b), we can observe a curvature in the resonant semimajor axis, a black dashed line, caused by the bifurcation of the resonance.

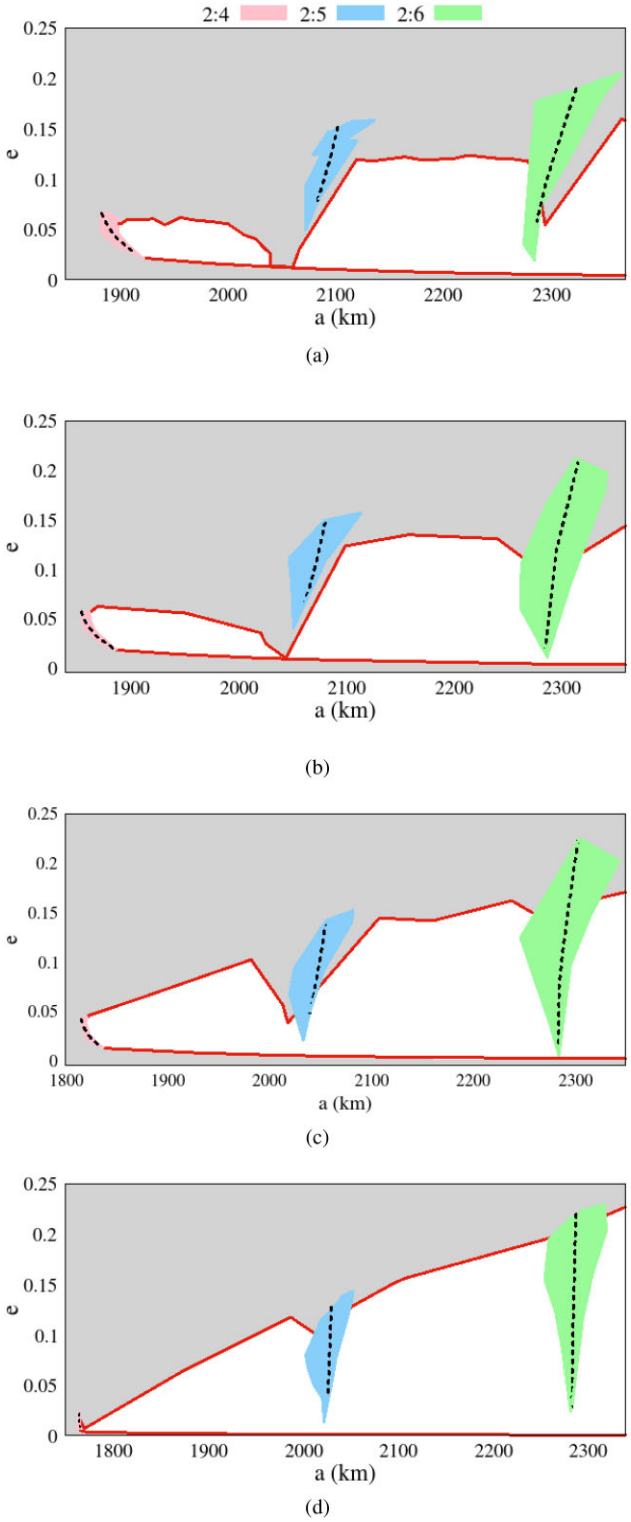

Figure 17. Maps of the stable and unstable regions in the $a - e$ space of the systems (a) Haumea, (b) Haumea^a, (c) Hamuea^b and (d) Haumea^c. Maps were obtained from the Poincaré surface of section. Particles with semi-major axis and eccentricity within the gray region either collide with the central body or are ejected. In the other regions, the particles remain stable for more than 10 000 orbits. The pink, blue and green regions are related to the 2:4, 2:5 and 2:6 resonances, respectively. The black dashed lines indicate the centres of each resonance determined by the geometry of the resonant orbits. The lower red line corresponds to the semi-major axis and eccentricity of first kind periodic orbits and the upper red line to quasi-periodic orbits.

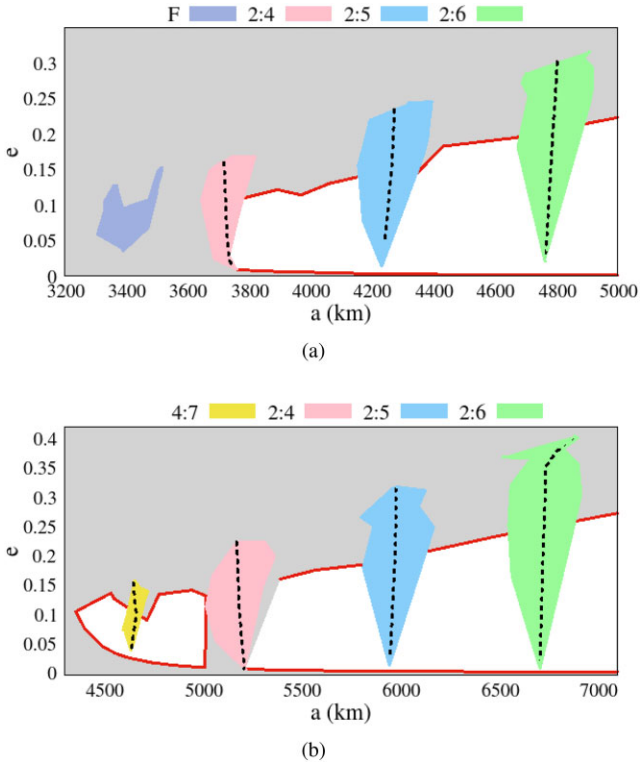

Figure 18. Maps of the stable and unstable regions in the *a*–*e* space of the systems (a) Haumea^{d} and (b) Haumea^{e}, obtained from the Poincaré surface of section. Particles with semimajor axis and eccentricity within the grey region either collide with the central body or are ejected. In the other regions, the particles remain stable for more than 10 000 orbits. The yellow, pink, blue, and green regions are related to the 4:7, 2:4, 2:5, and 2:6 resonances, respectively. The purple region in plot (a) refers to the F1 and F2 family. The black dashed lines indicate the centres of each resonance determined by the geometry of the resonant orbits. The lower red line corresponds to the semimajor axis and eccentricity of first kind periodic orbits and the upper red line to quasi-periodic orbits.

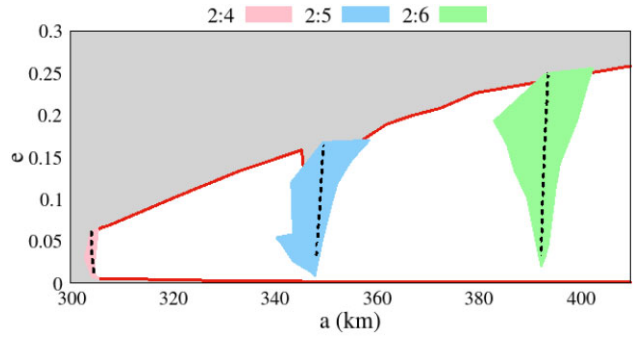

Figure 19. Map of the stable and unstable regions in the *a*–*e* space of the Chariklo system, obtained from the Poincaré surface of section. Particles with semimajor axis and eccentricity within the grey region either collide with the central body or are ejected. In the other regions, the particles remain stable for more than 10 000 orbits. The pink, blue, and green regions are related to the 2:4, 2:5, and 2:6 resonances, respectively. The black dashed lines indicate the centres of each resonance determined through the geometry of the resonant orbits. The lower red line corresponds to the semimajor axis and eccentricity of first kind periodic orbits and the upper red line to quasi-periodic orbits.

Changing systems again, Fig. 19 shows the mapping of the region around Chariklo. This centaur is considerably less elongated and rotates more slowly compared to Haumea. Consequently, the stable region (in white) is larger and without abrupt drops in eccentricity in the upper red line, associated with quasi-periodic orbits of the first kind. The width of the 2:4 resonance is narrower than the others. The orbits associated with the 2:6 resonance are more eccentric, with variations between $0.05 < e < 0.29$.

The maps presented in this section show the impact of the ellipticity and spin of the central body on the stable and unstable regions and, consequently, on the widths of the resonances. It is common to build the *a*–*e* maps through theoretical models using the circular restricted three-body problem. However, it was not possible to use this model in the systems analysed in this work, due to the difficulty in describing orbital elements of trajectories around prolate bodies. This disagreement between the analytical model and numerical results was pointed out in the work of Olsen (2006), who found discrepancies in the location of resonances close to the central body (see their figs 1, 3, 4, and 5).

5 APPLICATIONS: SPACECRAFT, RINGS, AND SATELLITES

In this study, we identified chaotic and stable regions around prolate bodies. Stability zones are associated with periodic and quasi-periodic orbits, some of them are resonant and some are not. These analyses can be used in several applications, such as space missions, natural satellites, or rings particle. Next, we present some of these applications.

Periodic orbits, resonant or non-resonant, have characteristic trajectories format, which is repeated over time as, for example, those shown in Figs 10 to 13. Identifying the location of periodic orbits can be advantageous for space missions, as that by placing a spacecraft on this trajectory it is possible to predict what its behaviour will be over time, in addition, the spacecraft will be inserted in a stable zone, since around periodic orbit there is a region of quasi-periodic orbits, as shown in Figs 4, 5, 6, and 7. Several works have been developed in the last decades in order to discover periodic orbits for space missions around smaller and irregular celestial bodies, as is the case of the work of Jiang et al. (2018) that explores this type of trajectory around the asteroids 243 Ida, 433 Eros, 6489 Golevka, 101 955 Bennu, and comet 1P/Halley.

Stable regions, linked to resonances or other periodic orbits, correspond to the birth environment of rings and satellites. Ring particles located in stable regions are expected to have long lifetimes in the absence of external perturbation, possibly giving rise to moons (Madeira, Charnoz & Hyodo 2023a; Madeira et al. 2023b). Satellites in stable regions, in turn, can give rise to rings, for example, by ejecting material due to external impacts (Madeira & Giuliatti Winter 2020, 2022). On the other hand, these regions can be dangerous for a space mission, as they can be populated by natural objects.

The *chaotic regions* are also interesting for spacecraft, they be an areas devoid of natural material. Over time, rings or moons that formed in the region are removed due to instability. In the systems studied in this work, we found an extensive region of chaos, for example, the region internal to the 2:4 resonance, as shown in the maps of Figs 17, 18, and 19. This is an area close to the body that becomes interesting for missions that seek to study its surface. Because they are in unstable zones, it is necessary to use some control mechanism to guide the spacecraft for the time stipulated by the mission.

6 CONCLUSIONS

In this work, we seek to present an analysis of the dynamics of the region around prolate bodies. For this, we used the Poincaré surface of section technique, which provided the necessary information for the identification of stable and unstable regions in the phase space of the seven considered systems. The central bodies were modelled by an ellipsoidal gravitational potential of an ellipsoidal body. Among these systems, we change the rotation period, ellipticity, and mass of the primary, to identify how the region around these bodies is affected by these physical parameters. Our results are summarized below:

(i) On the Poincaré surface of section, we identify the double resonances, which were pointed out in the works of Winter et al. (2019) and Sicardy (2020). In addition, in the Haumea^e system we identify the bifurcation of the 2:6 resonance. Analysing the Poincaré surface of section, we find that both the ellipticity of the central body and the spin affect the location of the resonances.

(ii) To measure the extent of stable and unstable regions, delimited by periodic and quasi-periodic orbits, we used the method discussed in Ribeiro et al. (2021). The use of epicyclic frequencies to calculate the semimajor axis of orbits around prolate bodies leads to inconsistencies with the numerical results for regions close to the central body. Such disagreements were also identified in the work of Olsen (2006), who compared numerical simulations with an analytical method (mean elements) for determining the width of spin-orbit resonances around prolate bodies.

(iii) Having defined the method to calculate the semimajor axis and eccentricity of the orbits, we build stability maps in the a–e space. With the maps, we identified that the widths of the resonances are not symmetrical about the centre of the resonance, defined by the resonant semimajor axis.

(iv) It was possible to identify a large region of stability, in semimajor axis and eccentricity, due to the first kind of orbits. Periodic orbits of the first kind, in general, have almost zero eccentricity and are present in a large semimajor axis interval for all studied systems, while resonant and quasi-periodic orbits have high eccentricities.

ACKNOWLEDGEMENTS

This study was financed in part by the Coordenação de Aperfeiçoamento de Pessoal de Nível Superior – Brasil (CAPES) – Finance Code 001, Fundação de Amparo á Pesquisa do Estado de São Paulo (FAPESP) – Proc. 2016/24561-0 and Proc. 2018/23568-6, Conselho Nacional de Desenvolvimento Científico e Tecnológico (CNPq) – Proc. 305210/2018-1 and Proc. 313043/2020-5. GM thanks to the Centre National d'Études Spatiales (CNES) and European Research Council (ERC). Finally, we thank the anonymous reviewer for the comments that significantly improved our work.

DATA AVAILABILITY

The data underlying this article will be shared on reasonable request to the corresponding author.

REFERENCES

Balmino G., 1994, Celest. Mech. Dyn. Astron., 60, 331
Bérard D. et al., 2017, AJ, 154, 144
Borderes-Motta G., Winter O. C., 2018, MNRAS, 474, 2452
Borderies N., Longaretti P. Y., 1987, Icarus, 72, 593
Borderies N., Longaretti P. Y., 1994, Icarus, 107, 129
Braga-Ribas F. et al., 2014, Nature, 508, 72
Broucke R., 1968, Technical Report: Periodic Orbits in the Restricted Three Body Problem with Earth-Moon Masses. Caltech, Pasadena
Chandrasekhar S., 1942, Principles of Stellar Dynamics. Dover, New York
Geissler P., Petit J.-M., Durda D. D., Greenberg R., Bottke W., Nolan M., Moore J., 1996, Icarus, 120, 140
Hénon M., 1965a, A&A, 28, 499
Hénon M., 1965b, A&A, 28, 992
Hénon M., 1966a, A&A, 29, 49
Hénon M., 1966b, A&A, 29, 57
Hénon M., 1969, Acad. Sci. Paris C. R. Ser. B - Sci. Phys., 269, 223
Hu W., Scheeres D., 2004, Planet. Space Sci., 52, 685
Jefferys W. H., 1971, Publications of the Department of Astronomy. The University of Texas at Austin, Austin, TX, USA
Jiang Y., Schmidt J. A., Li H., Liu X., Yang Y., 2018, Astrodynamics, 2, 69
Leiva R. et al., 2017, AJ, 154, 159
Longaretti P. Y., Borderies N., 1991, Icarus, 94, 165
Madeira G., Giuliatti Winter S. M., 2020, Eur. Phys. J.: Spec. Top., 229, 1527
Madeira G., Giuliatti Winter S. M., 2022, MNRAS, 513, 297
Madeira G., Giuliatti Winter S., Ribeiro T., Winter O., 2022, MNRAS, 510, 1450
Madeira G., Charnoz S., Hyodo R., 2023a, Icarus, 394, 115428
Madeira G., Charnoz S., Zhang Y., Hyodo R., Michel P., Genda H., Winter S. G., 2023b, AJ, 165, 161
Morgado B. et al., 2021, A&A, 652, A141
Mysen E., Aksnes K., 2007, A&A, 470, 1193
Mysen E., Olsen Ø., Aksnes K., 2006, Planet. Space Sci., 54, 750
Olsen Ø., 2006, A&A, 449, 821
Ortiz J. L. et al., 2017, Nature, 550, 219
Poincaré H., 1895, Gauthier-Villars et ls. Paris, 3, 414
Rabinowitz D. L., Barkume K., Brown M. E., Roe H., Schwartz M., Tourtellotte S., Trujillo C., 2006, AJ, 639, 1238
Ragozzine D., Brown M. E., 2009, AJ, 137, 4766
Renner S., Sicardy B., 2006, Celest. Mech. Dyn. Astron., 94, 237
Ribeiro T., Winter O., Mourão D., Boldrin L., Carvalho J., 2021, MNRAS, 506, 3068
Sicardy B., 2020, AJ, 159, 102
Sicardy B., Leiva R., Renner S., Roques F., El Moutamid M., Santos-Sanz P., Desmars J., 2019, Nat. Astron., 3, 146
Werner R. A., 1994, Celest. Mech. Dyn. Astron., 59, 253
Winter O. C., Murray C. D., 1994a, Atlas of the Planar, Circular, Restricted Three-Body Problem. I. Internal Orbits, Vol. 1. School of Mathematical Sciences, Queen Mary and Westfield College, London
Winter O. C., Murray C. D., 2, 1994b, Atlas of the Planar, Circular, Restricted Three-Body Problem. II. External Orbits. School of Mathematical Sciences, Queen Mary and Westfield College, London
Winter O. C., Murray C. D., 1997a, A&A, 319, 290
Winter O. C., Murray C. D., 1997b, A&A, 328, 399
Winter O., Neto E. V., 2002, A&A, 393, 661
Winter O. C., Borderes-Motta G., Ribeiro T., 2019, MNRAS, 484, 3765

This paper has been typeset from a TEX/LATEX file prepared by the author.